Hf thickness dependence of perpendicular magnetic anisotropy, damping and interfacial Dzyaloshinskii-Moriya interaction in Pt/CoFe/Hf/HfO_2

D. Ourdani,[1] Y. Roussigné,[1] R. B. Mos,[2] M. Nasui,[2] S. M. Chérif,[1] M. S. Gabor,[2,*] and M. Belmeguenai[1,†]

[1]*Université Sorbonne Paris Nord, LSPM, CNRS, UPR 3407, F-93430 Villetaneuse, France*

[2]*Center for Superconductivity, Spintronics and Surface Science, Physics and Chemistry Department, Technical University of Cluj-Napoca, Str. Memorandumului No. 28 RO-400114 Cluj-Napoca, Romania*

(Received 18 May 2021; revised 15 July 2021; accepted 27 July 2021; published 11 August 2021)

Vibrating sample magnetometery (VSM) combined with Brillouin light scattering (BLS) were used to investigate the Dzyaloshinskii-Moriya interaction (iDMI), the perpendicular magnetic anisotropy (PMA) and the damping in $Co_{0.5}Fe_{0.5}$-based systems grown by sputtering on Si/SiO_2 substrates, using Pt or Cu buffer layers and Hf capping layer of variable thickness ($0 \leqslant t_{Hf} \leqslant 2$ nm). VSM measurements revealed a significant decrease of the areal magnetic moment at saturation as t_{Hf} increases, most likely due to the increase of the magnetic dead layer thickness at CoFe/Hf interface up to 0.73 ± 0.06 nm for $t_{Hf} = 2$ nm. Damping measurements allowed concluding to the weaker spin pumping contribution by the CoFe/Hf interface compared to Pt/CoFe. The analysis of the t_{Hf} dependence of damping within a model considering the contribution of each interface allowed us to determine the spin diffusion length of Hf, found to be 1.7 nm. The Hf thickness dependence of iDMI and PMA constants revealed significant (weak) contribution of the CoFe/Hf interface to PMA (iDMI). The surface iDMI constant of CoFe/Hf interface was estimated to be $(-0.37 \pm 0.12) \times 10^{-7}$ erg/cm. This suggests that the iDMI sign of Hf and Pt are opposite, and an additive behavior can be obtained when they are placed in opposite sides of the CoFe layer, allowing thus to strengthen the iDMI, needed for some applications. Quadratic correlations between PMA and iDMI constants and linear dependence of damping versus PMA constant were obtained confirming their relationship with the spin-orbit coupling.

DOI: 10.1103/PhysRevMaterials.5.084404

I. INTRODUCTION

The interfacial Dzyaloshinskii-Moriya interaction (iDMI) [1], which is a spin-orbit coupling (SOC)-related antisymmetric exchange interaction between neighboring spins, is of great importance for the next-generation spintronic nonvolatile memory devices. Usually, the iDMI appears in heavy metal (HM)/ferromagnet (FM) bilayers due to the interfacial SOC and the broken symmetry. It can stabilize a variety of spin textures such as Néel-type domain walls (DWs) [2,3], spin spirals [4,5], and skyrmions [6,7] in ultrathin HM/FM bilayers. Moreover, the iDMI leads to fast DW motion driven by current induced spin-orbit torques and plays a critical role in the DW moving direction [8]. Besides iDMI, perpendicular magnetic anisotropy (PMA) can arise in such ultrathin film-based systems due to the surface anisotropy caused by the broken symmetry. PMA is crucial to enhance the thermal stability [9] and to reduce the critical current densities in spin transfer torque-based magnetic random-access memories (STT-MRAM) [10]. Moreover, as the FM thickness is reduced, damping, which is another key technological parameter controlling the magnetization dynamics, increases drastically due to spin pumping at the HM/FM interface thus affecting the DW speed and the switching current densities [11].

Skyrmions are stabilized by the interplay between iDMI and other interactions like symmetric exchange, dipolar coupling and PMA, and possessing a large iDMI energy density is a crucial requirement. However, based on numerical studies, Jang *et al.* [12] reported that the iDMI decreases the thermal energy barrier while it increases the switching current density and thus iDMI should be minimized for STT-MRAM applications. Therefore, simultaneously controlling the iDMI, damping, and PMA are needed for the design and the implementation of high speed skyrmion-based spin-orbitronic devices with dense integration and low energy cost. The strength of all these three phenomena is extremely sensitive to the thickness of the FM layer and to the interface quality affected by the surface roughness and the atomic intermixing. For example, to strengthen the iDMI, the structural inversion symmetry of a layered system has to be broken and the interface quality should tend to an ideal surface without any disorder. Therefore, the aim of this paper concerns the investigation of these three effects in Pt/CoFe/Hf/HfO_2 systems. The idea is to control their strength via optimizing the interface conditions through the introduction of an ultrathin intermediate layer of Hf of variable thickness and using additive effects from two materials with opposite iDMI. For this, Brillouin light scattering (BLS) coupled to vibrating sample magnetometer (VSM) techniques were used.

*mihai.gabor@phys.utcluj.ro

†belmeguenai.mohamed@univ-paris13.fr

II. SAMPLES AND EXPERIMENTAL TECHNIQUES

All the samples studied here, consisting mainly of Pt, Hf and $Co_{0.5}Fe_{0.5}$ (CoFe) stacks, are grown at room temperature (RT) using a magnetron sputtering system, having a base pressure lower than 2×10^{-8} Torr, on thermally oxidized Si/SiO_2 substrates. Three types of samples were grown: Si/SiO_2//Ta(2.5)/Pt(4)/CoFe(t_{CoFe})/Hf(t_{Hf})/HfO_2(2)/Ta(2.5), Si/SiO_2//Ta(2.5)/Pt(4)/Cu(3)/CoFe(1.4)/Hf(t_{Hf})/HfO_2(2)/Ta(2.5), and Si/SiO_2//Ta(2.5)/Hf(6)/CoFe(t_{CoFe})/HfO_2(2)/Ta(2.5) where the numbers in parentheses represent the thickness in nanometers, referred to as Pt/CoFe/Hf, Pt/Cu/CoFe/Hf and Hf/CoFe/HfO_2, respectively. The thickness of the CoFe layer (t_{CoFe}) is varied in the range of (0.6, 1 and 1.4 nm) for Pt/CoFe/Hf and between of 1 and 2.2 nm for Hf/CoFe/HfO_2, while that of the Hf layer (t_{Hf}) varies from 0 up to 2 nm. All the metallic films are dc sputtered in an Ar pressure of 1.5 mTorr, while the HfO_2 layer is rf sputtered under an Ar pressure of 3 mTorr from a ceramic target. No postgrowth annealing treatment was applied to samples. Pt is a heavy metal having high spin-orbit coupling which leads to large iDMI strength. Hf is a 5*d* heavy metal, less studied for iDMI and is expected to induce opposite iDMI sign [13] compared to Pt and therefore could lead to large iDMI when these two materials (Pt and Hf) are placed at either side of the ferromagnetic CoFe layer, as in the case of the first set of samples. For the second set of samples, Pt is decoupled from CoFe by a 3-nm-thick Cu interlayer to probe solely the effect of the upper CoFe/Hf interface on the properties of interest. For further comparison and to identify the effect of Hf/CoFe interface, Hf/CoFe/HfO_2 samples with 6-nm-thick Hf layer, sufficiently higher than its spin diffusion length [14], are used.

For all the samples, the hysteresis loops are measured under in-plane and perpendicular applied magnetic fields using a VSM and the magnetization at saturation (M_s) is then determined. BLS [15], under in-plane applied magnetic field, was used in Damon-Eshbach configuration to investigate iDMI, PMA, and damping. For this, the recorded spectra are fitted with Lorentzian to obtain the Stokes (S) and anti-Stokes (aS) line frequencies and their full width at half maximum (δF_S and δF_{aS}). For PMA and damping investigation, the field dependence of the mean frequency [$F = (F_S + F_{aS})/2$] and the mean linewidth δF[$\delta F = (\delta F_S + \delta F_{aS})/2$], at fixed spin wave vector of 8.08 μm^{-1} (incident angle of 20°), were used, respectively, whereas, the variation of the frequency mismatch between Stokes and anti-Stokes lines ($\Delta F = F_S - F_{aS}$) versus the spin wave vector (k_{sw}) allowed us to characterize the iDMI strength. All the measurements presented below were carried out at room temperature.

III. RESULTS AND DISCUSSIONS

To probe the crystal structure of the stacks, we performed x-ray diffraction experiments on selected samples. Figure 1(a) shows $2\theta/\omega$ diffraction patterns recorded for samples S1-Ta(2.5)/Pt(4)/CoFe(1.4)/Hf(6)/HfO_2(4), S2-Ta(2.5)/Pt(4)/CoFe(10)/Hf(6)/HfO_2(4), S3-Ta(2.5)/Hf(6)/CoFe(1.4)/HfO_2(4) and S4-Ta(2.5)/Hf(6)/CoFe(10)/HfO_2(4), where the numbers in parentheses represent the thickness in nanometers. In the

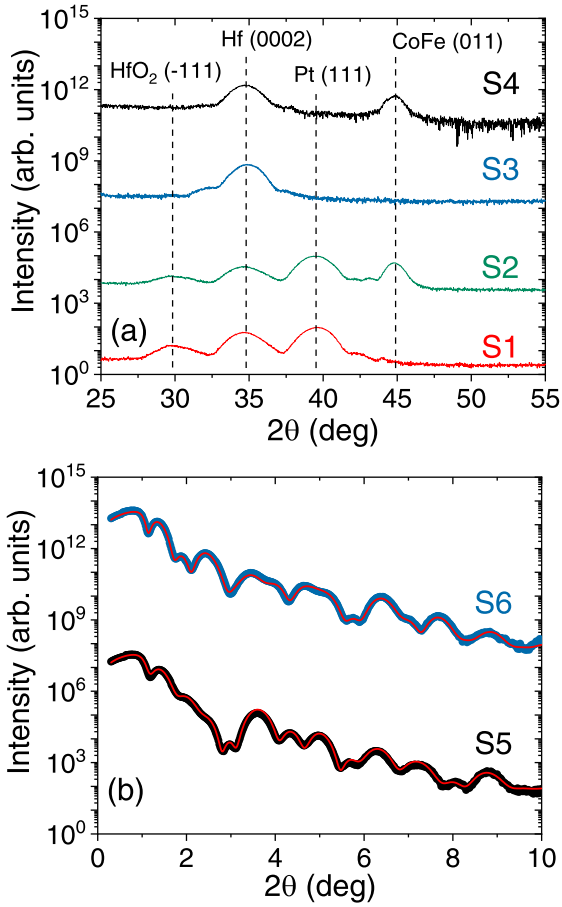

FIG. 1. (a) $2\theta/\omega$ diffraction patterns recorded for samples S1-Ta(2.5)/Pt(4)/CoFe(1.4)/Hf(6)/HfO_2(4), S2-Ta(2.5)/Pt(4)/CoFe(10)/Hf(6)/HfO_2(4), S3-Ta(2.5)/Hf(6)/CoFe(1.4)/HfO_2(4) and S4-Ta(2.5)/Hf(6)/CoFe(10)/HfO_2(4). (b) X-ray reflectivity patterns on samples S5-Ta(2.5)/Pt(4)/CoFe(1.4)/HfO_2(2)/Ta(2.5) and S6-Ta(2.5)/Pt(4)/CoFe(1.4)/Hf(1.5)/HfO_2(2)/Ta(2.5). Symbols are experimental data, while the continuous lines are theoretical fits within the Parratt formalism.

case of the S1 sample, the pattern shows the presence of the (111) reflection, of fcc-Pt, the (0002) of hcp- Hf, and the (-111) of m-HfO_2. Is worth mentioning that patterns recoded on a wider 2θ range do not show the presence of other peaks, except to the one corresponding to the Si substrate. No diffraction maxima belonging to the Ta buffer layer are visible, indicating that the film is in an amorphous or nanocrystalline state. Due to the ultralow thickness of the CoFe layer, corroborated with the relatively low atomic scattering factors of Co and Fe, no peaks issued from the CoFe are detected. Therefore, we deposited sample S2 with an increase CoFe layer thickness of 10 nm. Besides the peaks displayed also by the S1 sample, in the case of the S2 sample, the diffraction maxima corresponding to the (011) bcc-CoFe reflection is also observable. These results indicate that the Pt layer has a (111), Hf layer has a (002), while the CoFe layer has a (011) out-of-plane texture, confirmed also by ω-scan measurements (not shown here). The Pt is well known to grow with a strong (111) out-of-plane texture when deposited on amorphous Ta. It is conceivable that the texturing of the

Pt layer to induce the crystal texture of the CoFe and Hf upper layers. To test this hypothesis, we analysed sample S3 where the Hf layer is grown directly on the amorphous Ta layer. The diffraction pattern shows only the maxima corresponding to the (0002) Hf reflection, indicating that the texturing of the Hf layer takes place even in the absence of the (111) textured Pt underlayer. Similarly to the case of the S2 sample, the S4 sample with a CoFe layer of 10 nm shows also the (011) CoFe reflection, attesting to the out-of-plane texturing of the CoFe film when grown on Hf. As in our previous work [15], we tested a possible in-plane texturing of the stacks by performing ϕ-scan measurements and probed the (002) reflection of Pt (not shown here). No maxima were observed during the ϕ-scan suggesting an in-plane isotropic distribution of the Pt crystallites, which is expected having in view that the Pt film is grown on an amorphous underlayer. The in-plane isotropic distribution of the CoFe crystallites was confirmed by VSM measurements of the remanent magnetization after saturation at different in-plane angles showing a slightly uniaxial character, which is typical for sputtered films. It is worth to mention that the S1 and S2 samples diffraction patterns show the presence the (-111) of HfO_2 reflection, while it is absent in the case of the S3 and S4 samples. This indicates that the HfO_2 film grows out-of-plane textured when deposited on textured metallic Hf, confirmed also by ω-scan measurements (not shown here).

As we will argue below, one key feature in understanding our results is the atomic intermixing at the CoFe/Hf interface. To characterize the possible intermixing, we performed x-ray reflectivity measurements on two samples S5-Ta(2.5)/Pt(4)/CoFe(1.4)/HfO_2(2)/Ta(2.5) and S6-Ta(2.5)/Pt(4)/CoFe(1.4)/Hf(1.5)/HfO_2(2)/Ta(2.5), shown in Fig. 1(b) alongside with the fits to the experimental data within the Parratt formalism. As ca be seen from Fig. 1(b), the relatively long attenuation length and low oscillations decay at higher angles indicates overall low roughness and good interface sharpness. In the case of the S5 sample, the thickness of the CoFe layer obtained after fitting the reflectivity pattern, was 1.46 ± 0.14 nm, close to the nominal thickness of 1.4 nm. Interestingly, in the case of the S6 sample, fitting the reflectivity data gives a thickness for the CoFe of 0.75 ± 0.25 nm and for the Hf layer of a 2.19 ± 0.23 nm, together with a decrease of about 10% of the film density relative to the nominal one. One should mention that within the error bars all the other fitting parameters of all the layers remain the same as for sample S5. The thickness decrease of the CoFe layer and the thickness increase of the Hf layer, relative to the nominal values, is a clear indication of the intermixing that takes place at the CoFe/Hf interface.

The magnetic moment at saturation (m_s) for Pt/CoFe(t_{CoFe})/Hf(t_{Hf}) and Pt/Cu/CoFe(1.4 nm)/Hf(t_{Hf}) was measured by VSM and the corresponding nominal magnetizations at saturation (M_{sn}) were calculated by dividing m_s to the nominal volume of the CoFe film, as shown in Fig. 2(a). M_{sn} decreases with increasing t_{Hf} for both systems most probably due to increasing intermixing at the CoFe/Hf interface. Indeed, due to their larger atomic weight, heavy atoms such Pt and Hf are more energetic than light atoms such Cu and are expected to diffuse more in CoFe layer leading to higher interface mixing, when they are grown on the top of CoFe. In contrast, when the CoFe layer is grown on the top of the heavy metal the intermixing at the interface is reduced. The higher M_{sn} values for Pt/CoFe/Hf(t_{Hf}) compared to Pt/Cu/CoFe/Hf(t_{Hf}) over the whole t_{Hf} range can be attributed to the proximity induced magnetization (PIM) at Pt/CoFe

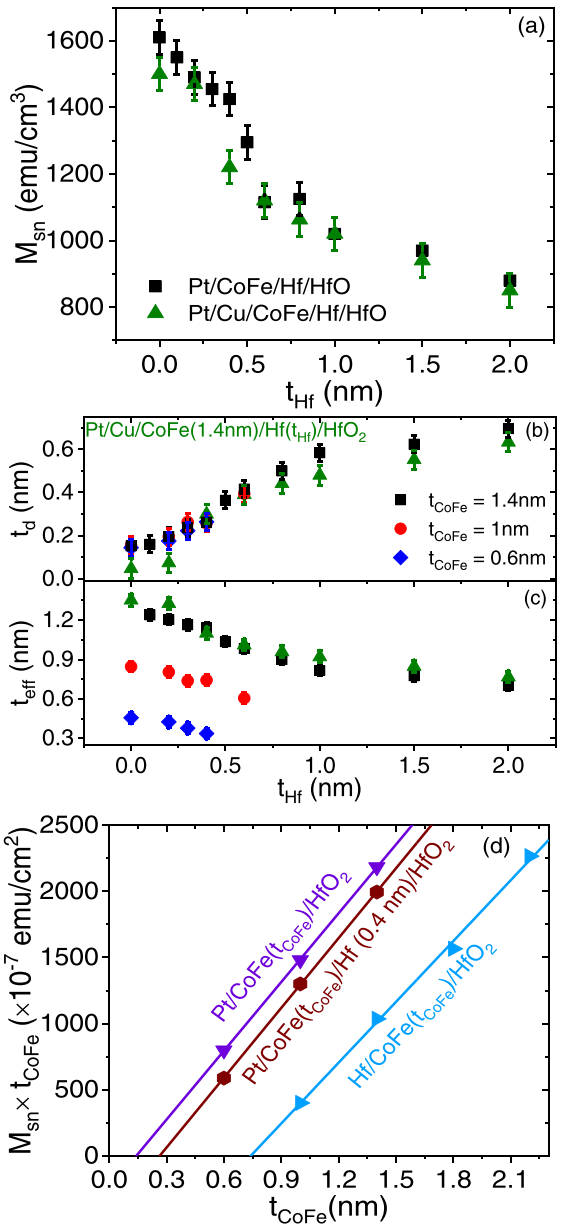

FIG. 2. (a) Variations of the nominal magnetization at saturation (M_{sn}), calculated by dividing the measured VSM magnetic moment at saturation to the nominal volume (surface × nominal thickness of CoFe) of the CoFe film for Pt/CoFe(1.4 nm)/Hf(t_{Hf}) and Pt/Cu/CoFe(1.4 nm)/Hf(t_{Hf}), versus the Hf thickness (t_{Hf}). (b) Magnetic dead thickness (t_d), deduced from the measured M_{sn} by considering that M_{sn} is given by $M_{sn} \times t_{CoFe} = M_s \times (t_{CoFe} - t_d)$ and (c) effective CoFe thickness ($t_{eff} = t_{CoFe} - t_d$), where $t_{CoFe} = 1.4$, 1, or 0.6 nm, versus the Hf thickness (t_{Hf}). (d) Saturation magnetic moment per unit area versus CoFe thickness of Pt/CoFe(t_{CoFe})/HfO_2, Pt/CoFe(t_{CoFe})/Hf(0.4 nm) and Hf/CoFe(t_{CoFe})/HfO_2. Symbols refer to the VSM measurements and solid lines are the linear fits.

interface. The similar extent variation of M_{sn} for both systems suggests the negligible intermixing at Pt/CoFe and Cu/CoFe interfaces compared to CoFe/Hf. To quantify the intermixing degrees, we determined the magnetic dead thickness for each t_{Hf} by considering that the measured nominal M_{sn} is given by $M_{sn} \times t_{CoFe} = M_s \times (t_{CoFe} - t_d)$, where $t_{CoFe} = 1.4$ nm. The Hf thickness dependence of t_d, shown in Fig. 2(b) and calculated for $M_s = 1750 \pm 20$ and 1550 ± 55 emu/cm^3 for Pt/CoFe/Hf(t_{Hf}) and Pt/Cu/CoFe/Hf(t_{Hf}), respectively, increases monotonously with t_{Hf} and shows a slower variation for $t_{Hf} > 1$ nm. t_d values of Pt/Cu/CoFe/Hf(t_{Hf}) at each t_{Hf} are slightly lower than those of Pt/CoFe/Hf(t_{Hf}) suggesting the lower (or even the negligible) intermixing at the Cu/CoFe compared to Pt/CoFe, as explained above. The corresponding values of the effective thickness of CoFe, defined as $t_{eff} = t_{CoFe} - t_d$, are shown in Fig. 2(c). The used $M_s(1750 \pm 20$ emu/cm^3) value in the estimation of t_d for Pt/CoFe/Hf(t_{Hf}) system was obtained from the linear fit of the CoFe layer thickness dependence of the areal magnetic moment at saturation ($M_{sn} \times t_{CoFe}$) shown in Fig. 2(d) for uncapped ($t_{Hf} = 0$) and 0.4-nm-thick Hf layer capped samples. This obtained value of M_s is in good agreement with the reported value by Pai *et al.* for Pt/Co/MgO (1720 ± 70 emu/cm^3) [16]. It is worth mentioning that the obtained values of t_d from the linear fit $M_{sn} \times t_{CoFe}$ for $t_{Hf} = 0 (t_d = 0.14 \pm 0.01$ nm), partially due to the oxidation of the CoFe layer when HfO_2 is deposited on top, and for $t_{Hf} = 0.4$ nm ($t_d = 0.24 \pm 0.01$ nm) are in good agreement with those presented in Fig. 2(b), deduced from the t_{Hf} dependence of M_{sn}. Similarly, t_d of Pt/Cu/CoFe/Hf(t_{Hf}) was estimated using the M_s value (1550 ± 55 emu/cm^3) obtained from the thickness dependence of $M_{sn} \times t_{CoFe}$ for Hf/CoFe/HfO_2, shown in Fig. 2(d), since no proximity induced magnetization (PIM) is expected from the Hf/CoFe interface. Moreover, the obtained value of $t_d (0.73 \pm 0.06$ nm) for Hf/CoFe/HfO_2 is of the same order as that corresponding for $t_{Hf} = 2$ nm in the Pt/CoFe/Hf(t_{Hf}) and Pt/Cu/CoFe/Hf(t_{Hf}) systems. This confirms again that the magnetic dead layer originates mainly from Hf/CoFe interface and that both upper and lower Hf layers produce significant intermixing with CoFe. It is also worth mentioning that the lower M_s value (1550 ± 55 emu/cm^3) for Hf/CoFe/HfO_2 compared to Pt/CoFe/Hf, corresponds to a change in CoFe magnetization of 13%, confirming the PIM at Pt/CoFe, since no PIM is expected from Hf/CoFe interface. Furthermore, the estimated t_d from VSM measurements on Pt/CoFe(1 nm)/Hf(t_{Hf}) and Pt/CoFe(0.6 nm)/Hf(t_{Hf}) for small t_{HF} are in good agreement with those of Pt/CoFe(1.4 nm)/Hf(t_{Hf}), as shown in Fig. 2(b), confirming the validity of above procedure for t_d estimation. In the following and for clarity, the Hf thickness effect will be transferred to the corresponding effective CoFe thickness

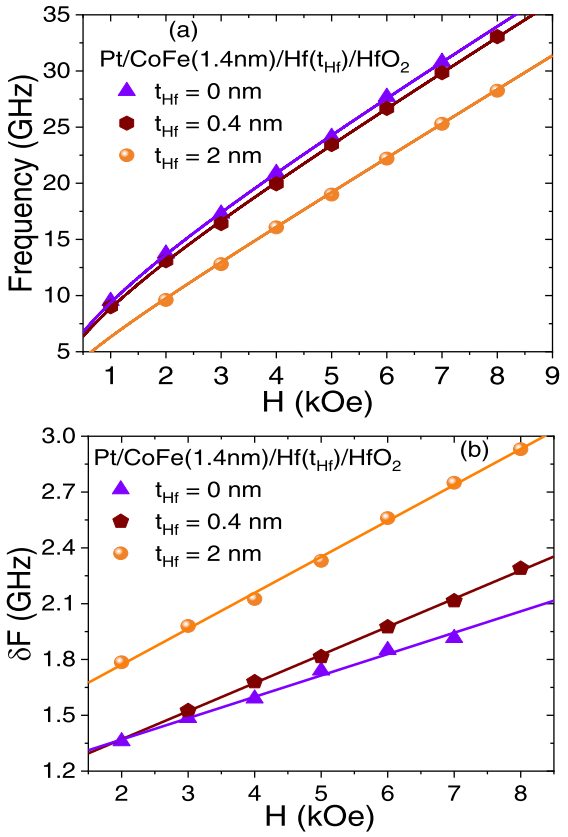

FIG. 3. Variations of the (a) the mean frequency [$F = (F_S + F_{aS})/2$] and (b) the mean δF[$\delta F = (\delta F_S + \delta F_{aS})/2$], determined from the fit of the recorded BLS spectra at fixed spin wave vector of 8.08 μm^{-1} (incident angle of 20°) to obtained the Stokes (S) and anti-Stokes (aS) line frequencies and their full width at half maximum (δF_S and δF_{aS}), for Pt/CoFe(1.4 nm)/Hf(t_{Hf}). Symbols refer to the experimental data and solid lines are fits using Eqs. (1) and (2).

defined as $t_{eff} = t_{CoFe} - t_d$ [see Fig. 2(c)], where t_d is shown in Fig. 2(b) for each t_{Hf}. To simplify the discussion of the observed trends, all parameters will be presented as a function of the effective thickness, unless it is explicitly mentioned.

We will now focus on the perpendicular magnetic anisotropy and the Gilbert damping. They can be determined from the field dependence of spin waves frequency through the investigation of the thickness dependence of the effective magnetization (M_{eff}) and from the field dependence of δF, respectively. Figure 3 shows the typical field dependences of F and δF for some selected samples compared to the best fits using Eqs. (1) and (2):

$$F = \frac{\gamma}{2\pi}\sqrt{\left[H + Jk_{sw}^2 + P(k_{sw}t_{eff})4\pi M_s\right]\left[H + Jk_{sw}^2 - P(k_{sw}t_{eff})4\pi M_s + 4\pi M_{eff}\right]}, \quad (1)$$

where H is the in-plane applied field, t_{eff} is the effective CoFe thickness, $J = \frac{2A_{ex}}{M_s}$ with A_{ex} is the exchange stiffness constant of CoFe, $\gamma/(2\pi) = 30$ GHz/T is the gyromagnetic ratio, and $P(k_{sw}t_{eff})$ is defined as in Ref. [17];

$$\delta F = \delta F_0 + \frac{\gamma}{2\pi} 2\alpha H, \quad (2)$$

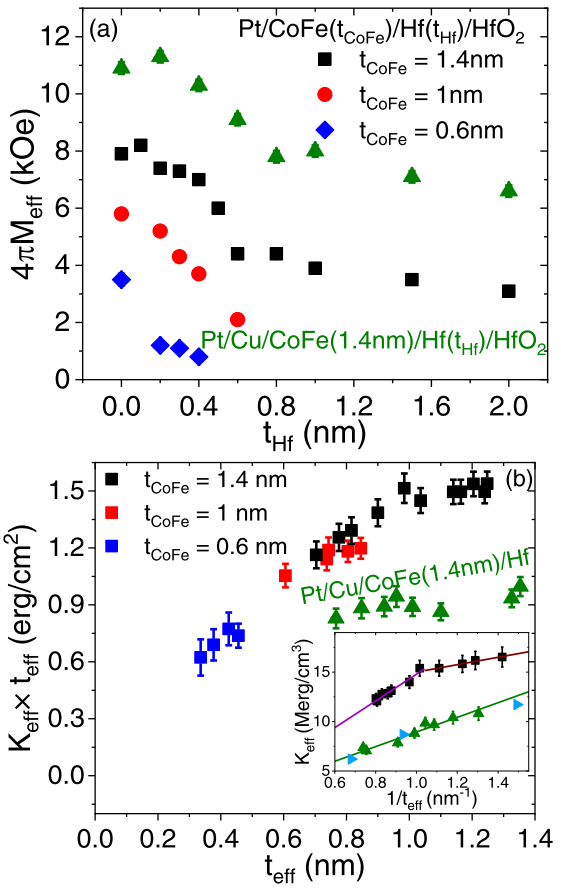

FIG. 4. Variations of the (a) effective magnetization ($4\pi M_{\rm eff}$) versus the Hf thickness and (b) the effective perpendicular anisotropy constant ($K_{\rm eff}$) times the effective thickness $K_{\rm eff} \times t_{\rm eff}$ versus the effective thickness of the CoFe layers ($t_{\rm eff}$) for Pt/CoFe($t_{\rm CoFe}$)/Hf($t_{\rm Hf}$) and Pt/Cu/CoFe(1.4 nm)/Hf($t_{\rm Hf}$) systems. $4\pi M_{\rm eff}$ values were extracted from the fit of similar measurements of Fig. 2(a). The inset in (b) shows the effective perpendicular anisotropy constant versus the inverse of the effective thickness of the CoFe layers for Pt/CoFe(1.4 nm)/Hf($t_{\rm Hf}$), Pt/Cu/CoFe(1.4 nm)/Hf($t_{\rm Hf}$) and Hf/CoFe($t_{\rm CoFe}$)/HfO_2 (blue triangles) systems. The effective CoFe thickness defined as $t_{\rm eff} = t_{\rm CoFe} - t_d$, where $t_{\rm CoFe} = 1.4$ nm and t_d is presented in Fig. 2(b) for each $t_{\rm Hf}$, in the case of Pt/CoFe(1.4 nm)/Hf($t_{\rm Hf}$) and Pt/Cu/CoFe(1.4 nm)/Hf($t_{\rm Hf}$). Symbols refer to experimental data while solid lines are the linear fits.

where δF_0 is the inhomogeneous residual linewidth and α is the Gilbert damping.

The obtained values of $4\pi M_{\rm eff}$ from the fit of the experimental data [displayed in Fig. 3(a)] are shown in Fig. 4(a) versus $t_{\rm Hf}$. For all systems, $M_{\rm eff}$ decreases with increasing Hf thickness, which would suggest increase of the perpendicular effective anisotropy field. Indeed, as mentioned above, the increase of Hf thickness induces further intermixing and thus enhances the magnetic dead layer and therefore, the effective magnetic thickness of CoFe decreases leading to higher PMA due to the interface anisotropy. Here, again, the inserted Cu layer between Pt and CoFe reduced the PMA resulting in a higher $M_{\rm eff}$ of Pt/Cu/CoFe/Hf($t_{\rm Hf}$) than those of Pt/CoFe/Hf($t_{\rm Hf}$). For further analysis of the observed trend, the effective PMA constant $K_{\rm eff}$ was calculated from $4\pi M_{\rm eff}$ ($4\pi M_{\rm eff} = 4\pi M_s - 2K_{\rm eff}/M_s$), using the above-mentioned M_s values inferred from the VSM measurements. Note that $K_{\rm eff}$ is usually described by the phenomenological relationship $K_{\rm eff} = K_v + \frac{K_s}{t_{\rm eff}}$, where K_s and K_v are the perpendicular uniaxial surface and volume anisotropy constants, respectively. Figure. 4(b) shows the effective anisotropy times the effective thickness $K_{\rm eff} \times t_{\rm eff}$ versus the effective thickness of the CoFe layers for Pt/CoFe($t_{\rm CoFe}$)/Hf($t_{\rm Hf}$), Pt/Cu/CoFe(1.4 nm)/Hf($t_{\rm Hf}$) and Hf/CoFe/HfO_2, where two regimes can be distinguished, in particular for Pt/CoFe($t_{\rm CoFe}$)/Hf($t_{\rm Hf}$). The increase of $K_{\rm eff}$ with thickness in both regimes is consistent with the decrease of the CoFe effective thickness as $t_{\rm Hf}$ increases, as mentioned above. The inset of Fig. 4(b) shows $K_{\rm eff}$ over a narrow $1/t_{\rm eff}$ range ($0.7\ {\rm nm} < 1/t_{\rm eff} < 1.3\ {\rm nm}$) for Pt/CoFe/Hf($t_{\rm Hf}$), where the two linear regimes with different slopes are more observable. Strain resulting from the nonmatching lattice parameters of CoFe and adjacent layers could lead to the existence of these two regimes, where for thinner films below a critical thickness the same in-plane lattice parameter is adopted as the adjacent layers (coherent regime) and when thickness overpasses the critical value the strains are partially relaxed (incoherent regime) through formation of misfit dislocations [18]. Several other mechanisms may also produce these two regimes, such as interface degradation, formation of different crystalline phases triggered by intermixing or the decrease of the Curie temperature when the CoFe thickness decreases. However, it is not possible to identify the precise mechanism or the combination of mechanisms behind these two regimes behavior and we may only speculate that it is due to strains relaxation and interface quality degradation. In the regime of thicker CoFe ($t_{\rm eff} > 1$ nm), the linear fits allowed us to derive $K_s = (1.35 \pm 0.13)\ {\rm erg/cm^2}$ and $K_v = (1.28 \pm 0.12) \times 10^6\ {\rm erg/cm^3}$. The deduced values of $K_s = (0.36 \pm 0.04)\ {\rm erg/cm^2}$ and $K_v = (1.13 \pm 0.04) \times 10^7\ {\rm erg/cm^3}$ in thinner CoFe ($t_{\rm eff} < 1$ nm) revealed drastic decrease of the surface anisotropy, most likely due to the degradation of thinner CoFe layers, the resulting lower Curie temperature or even diffusion of Hf up to the Pt/CoFe interface. The regime of thinner (thicker) CoFe layers is characterized by a strong (weak) volume PMA. For the Pt/Cu/CoFe(1.4 nm)/Hf($t_{\rm Hf}$) system, due to narrower available CoFe effective thickness, only the regime of thicker CoFe was characterized, where a $K_s = 0.74 \pm 0.07\ {\rm erg/cm^2}$ and a $K_v = (1.54 \pm 0.07) \times 10^6\ {\rm erg/cm^3}$ is observed. The obtained values of $K_{\rm eff}$ for Hf/CoFe($t_{\rm CoFe}$)/HfO_2 coincide perfectly with those of Pt/Cu/CoFe(1.4 nm)/Hf($t_{\rm Hf}$), suggesting that PMA originates mainly from the Hf/CoFe interface and Cu/CoFe induces a negligible interface PMA. Note the comparable K_v values in this regime for Pt and Cu buffered CoFe and the lower K_s compared to that of Pt/CoFe/Hf($t_{\rm Hf}$), suggesting that the surface anisotropy is partially induced by the Pt/CoFe interface. It is also worth mentioning that this regime of thicker CoFe films is observable over a larger range thickness for Pt/Cu/CoFe(1.4 nm)/Hf($t_{\rm Hf}$), suggesting that is correlated to strain in the coherent and incoherent growth regime. This agrees with the fact that the critical thickness (CoFe thickness separating the two regimes) should decrease as the lattice mismatch increases: i.e., the

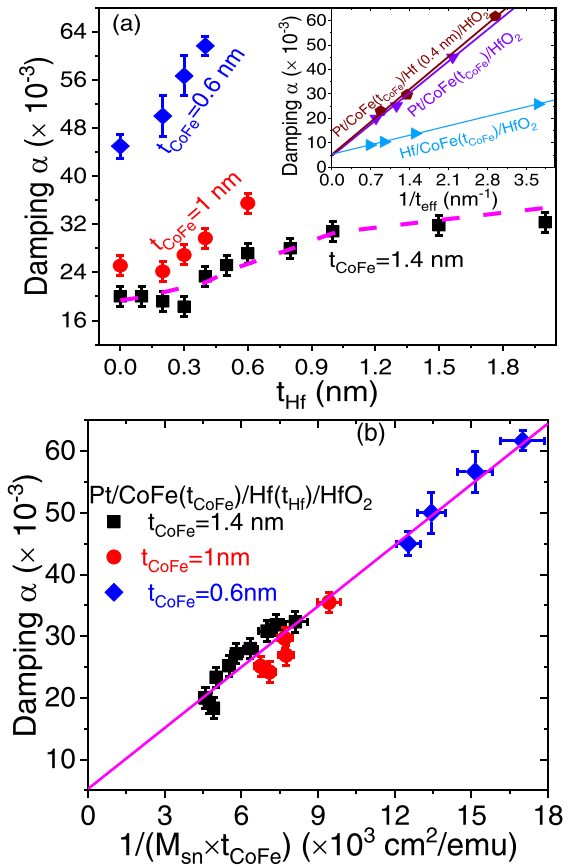

FIG. 5. (a) Variations of the Gilbert effective damping (α) versus the Hf thickness for Pt/CoFe($t_{\rm CoFe}$)/Hf($t_{\rm Hf}$) system. The inset shows α versus the inverse of the effective thickness of the CoFe layers for Pt/CoFe($t_{\rm CoFe}$)/HfO_2, Pt/CoFe($t_{\rm CoFe}$)/Hf(0.4 nm) and Hf/CoFe($t_{\rm CoFe}$)/HfO_2 systems. Symbols are experimental data and solid lines are linear fits whereas dashed line refers to fit using Eq. (4). (b) Variations of the Gilbert effective damping (α) versus $1/(M_s \times t_{\rm eff})$ for Pt/CoFe($t_{\rm CoFe}$)/Hf($t_{\rm Hf}$) system. Symbols are experimental data and dashed line is the fit using Eq. (4).

critical thickness of Pt/Cu/CoFe(1.4nm)/Hf($t_{\rm Hf}$)/HfO_2 is lower than that of Pt/CoFe(1.4nm)/Hf($t_{\rm Hf}$)/HfO_2. The lattice mismatches between Pt(111), Cu(111) and CoFe (011) are found to be around 10% and 3%, owing to the lattice constants of Pt ($a = 0.3912$ nm), Cu ($a = 0.3615$ nm) and CoFe ($a = 0.2855$ nm). As also mentioned above, these two regimes could also result from the formation of different crystalline phases triggered by intermixing, or the interface quality degradation which is lesser for Pt/Cu/CoFe(1.4 nm)/Hf($t_{\rm Hf}$). Indeed, as the Hf thickness increases the intermixed Hf reaches the bottom interface. This has a stronger effect in the case of Pt/CoFe since the Pt/CoFe interface contributes significantly in K_s. Conversely, it has a negligible effect for Cu/CoFe since this interface does not produce K_s.

Figure. 5(a) shows the Hf thickness dependence of the Gilbert damping deduced from the fit of the field dependence of BLS linewidth [depicted in Fig. 3(b)], using Eq. (2) for Pt/CoFe(0.6, 1 and 1.4 nm)/Hf($t_{\rm Hf}$). α increases strongly with $t_{\rm Hf}$ for $t_{\rm Hf} \leqslant 0.6$ nm and then saturates for higher Hf thickness. It is worth mentioning that the increase of α with the decreasing CoFe thickness is at fixed $t_{\rm HF}$. These trends are most likely due to the spin pumping contribution to damping at Pt/CoFe and CoFe/Hf. In fact, the variation of Hf thickness results in two effects on spin pumping: (i) as $t_{\rm Hf}$ increases, the magnetic dead layer thickness increases reducing the effective thickness of CoFe, leading to higher damping due to spin pumping at the Pt/CoFe and CoFe/Hf; (ii) the dependence of the damping on the nonmagnetic metallic (NM) buffer or capping layer thickness (Pt or Hf here) can be described by Eq. (3) [19]:

$$\alpha = \alpha_{\rm CoFe} + \frac{g\mu_B}{4\pi M_s t_{\rm eff}} g_{\rm eff}^{\uparrow\downarrow} \left[1 - e^{-\frac{2t_{\rm NM}}{\lambda_{\rm SD}}}\right], \qquad (3)$$

where μ_B is the Bohr magneton, $\alpha_{\rm CoFe}$ is the Gilbert damping constant of the CoFe, g is the Landé factor, $\lambda_{\rm SD}$ is the spin diffusion length of the adjacent NM, $t_{\rm NM}$ is the thickness of the NM, and $g_{\rm eff}^{\uparrow\downarrow}$ is the effective spin mixing conductance. As $t_{\rm Hf}$ increases, the contribution of the CoFe/Hf interface to damping increases rapidly as shown in Fig. 5(a). To confirm the origin of the damping behavior, the variation of α as a function of $1/t_{\rm eff}$ is shown in the inset of Fig. 5(a) for $t_{\rm HF} = 0$ and 0.4 nm. Note the linear dependence of α versus $1/t_{\rm eff}$ with a slight variation of the slope with $t_{\rm Hf}$, suggesting that the damping increase is mainly induced by spin pumping at the Pt/CoFe interface. We thus consider that the total damping is given by $\alpha = \alpha_{\rm CoFe} + \alpha_P$ as described by Eq. (3). Due to the large Pt thickness (4 nm) compared to its spin diffusion length ($\lambda_{\rm SD} \approx 1$ nm) [20], the $e^{-\frac{2t_{\rm NM}}{\lambda_{\rm SD}}}$ is negligible in Eq. (3) and therefore, the damping introduced by the spin pumping effect due Pt/CoFe for $0 \leqslant t_{\rm Hf} < 0.4$ nm is given by $\alpha_P = \frac{g\mu_B}{4\pi M_s t_{\rm eff}} g_{\rm eff}^{\uparrow\downarrow}$. The linear fit of the experimental data gives $\alpha_{\rm CoFe} = (5.3 \pm 0.2) \times 10^{-3}$, which is in good agreement with the reported value of CoFe [21], and allows the determining of $g_{\rm eff}^{\uparrow\downarrow} = (20.4 \pm 2.0)$ nm^{-2} and (20.8 ± 1.2) nm^{-2} for $t_{\rm HF} = 0$ and 0.4 nm, respectively, which are in line with the reported value (25 nm^{-2}) by Li *et al.* [22]. This suggests the weaker contribution of the CoFe/Hf interface to spin pumping compared to Pt/CoFe for such thin Hf layers. To estimate the contribution of CoFe/Hf to spin pumping, the CoFe effective thickness dependence of damping for Hf/CoFe/HfO_2 systems is shown in the inset of Fig. 5(a). α varies linearly versus $1/t_{\rm eff}$ allowing the deduction of $\alpha_{\rm CoFe} = (5.3 \pm 0.2) \times 10^{-3}$ and $g_{\rm eff}^{\uparrow\downarrow} = (5.5 \pm 0.1)$ nm^{-2} for CoFe/Hf, effective spin mixing conductance much lower than that of Pt/CoFe.

Equation (3) indicates that the spin pumping introduced damping depends on $M_s \times t_{\rm eff}$. Due to the lack of precise values of the magnetic dead layer and thus $t_{\rm eff}$, it is more convenient to investigate this damping versus $M_s \times t_{\rm eff}$, which is directly measured by VSM by dividing the magnetic moment by the sample surface. Therefore, to further investigate the Hf thickness damping dependence and for a precise characterization of the spin pumping contribution, the total damping α is shown in Fig. 5(b) as a function of $1/(M_s \times t_{\rm eff})$, where a linear dependence is obtained, especially for Pt/CoFe($t_{\rm CoFe}$)/Hf($t_{\rm Hf}$) with thinner Hf layers (below 0.4 nm). Note the good agreement between data involving both variable $t_{\rm CoFe}$ and $t_{\rm Hf}$. Indeed, and as mentioned above, due to the double effect of $t_{\rm Hf}$ on the spin pumping induced damping, exponential and $1/t_{\rm eff}$ linear dependences are expected as $t_{\rm Hf}$

varies. Therefore, the presence of this double effect leads to a linear dependence versus $1/(M_s \times t_{\text{eff}})$ for $t_{\text{Hf}} < 0.4$ nm, where the CoFe/Hf contribution is weak, and to lesser linear dependence quality for the thicker Hf, due to the exponential contribution of CoFe/Hf. The linear dependence of α versus $1/(M_s \times t_{\text{eff}})$ allows us to deduce $g_{\text{eff}}^{\uparrow\downarrow} = (21 \pm 2)\ \text{nm}^{-2}$ and $\alpha_{\text{CoFe}} = (5.3 \pm 0.2) \times 10^{-3}$ for Pt/CoFe(t_{CoFe})/Hf(t_{Hf}), which are in good agreement with those obtained above from the $1/t_{\text{eff}}$ analysis. Moreover, to take into account the effect of t_{Hf} on damping, the experimental data of Fig. 5 for Pt/CoFe(1.4 nm)/Hf(t_{Hf}) were fitted with Eq. (4):

$$\alpha = \alpha_{\text{CoFe}} + \frac{g\mu_B}{4\pi M_s t_{\text{eff}}} g_{\text{Pt/CoFe}}^{\uparrow\downarrow} + \frac{g\mu_B}{4\pi M_s t_{\text{eff}}} g_{\text{CoFe/Hf}}^{\uparrow\downarrow}\left[1 - e^{-\frac{2t_{\text{Hf}}}{\lambda_{\text{SD}}}}\right], \quad (4)$$

where the contributions of each interface and their variation with t_{Hf} are considered. Using the above-mentioned values of $\alpha_{\text{CoFe}} = 5.3 \times 10^{-3}$, $g_{\text{Pt/CoFe}}^{\uparrow\downarrow} = 20.4\ \text{nm}^{-2}$ and $g_{\text{CoFe/Hf}}^{\uparrow\downarrow} = 5.5\ \text{nm}^{-2}$, where the λ_{SD} of Hf was determined to be 1.7 nm, which is in good agreement with the reported value by Pai *et al.* [14].

We will now focus on the iDMI, which can be determined through the investigation of the frequency mismatch ΔF, shown in Fig. 6(a) for $k_{\text{sw}} = 20.45\ \mu\text{m}^{-1}$. ΔF is significantly reduced by inserting Cu between Pt and CoFe and shows slight variation with t_{Hf}. Interestingly, ΔF behaves differently versus t_{Hf} for thin and thick CoFe: while for $t_{\text{CoFe}} = 1$ and 1.4 nm ΔF increases in absolute value with t_{Hf} up to 1 nm and then saturates for thicker Hf layers, it decreases with increasing t_{Hf} for $t_{\text{CoFe}} = 0.6$ nm. This difference could be explained by the degradation of the interface quality of the thinner CoFe layers. Moreover, for the thickest CoFe layer (1.4 nm), a significant increase (in absolute value) is observed: ΔF doubles its value when t_{HF} increases up to 1 nm. This increase cannot only originate from the CoFe/Hf interface. Indeed, while additional iDMI is expected from CoFe/Hf interface due to its opposite sign compared to that of CoFe/Pt, the strength of the additional iDMI is not coherent with the expected weak iDMI constant induced by Hf [13]. Therefore, this iDMI increase is most probably due to the additional contribution from the reduced effective thickness for CoFe as t_{HF} increases. To get more insight in the iDMI evolution, the frequency mismatch was measured versus k_{sw} and the iDMI effective constant D_{eff} was determined using Eq. (5):

$$\Delta F = D_{\text{eff}} \frac{2\gamma}{\pi M_s} k_{\text{sw}} = D_s \frac{2\gamma}{\pi M_s t_{\text{eff}}} k_{\text{sw}}, \quad (5)$$

where $D_{\text{eff}} = D_s/t_{\text{eff}}$ and D_s are the iDMI effective and surface constants, characterizing the iDMI strength.

For each sample, ΔF was measured versus k_{sw} (not shown here) and fitted with Eq. (5) using the M_s values mentioned above [1750 emu/cm^3 for Pt/CoFe/Hf(t_{Hf}) and 1550 emu/cm^3 for Pt/Cu/CoFe/Hf(t_{Hf})] to determine D_{eff} as shown in Fig. 6(b). The Pt/CoFe(0.6 nm)/Hf(t_{Hf}) system stands out remarkably from the other structures: while D_{eff} of all the other systems increases in absolute values with t_{Hf} (thus decreasing t_{eff}), D_{eff} decreases as t_{Hf} increases. This decrease of D_{eff} is most likely due to the fact that iDMI

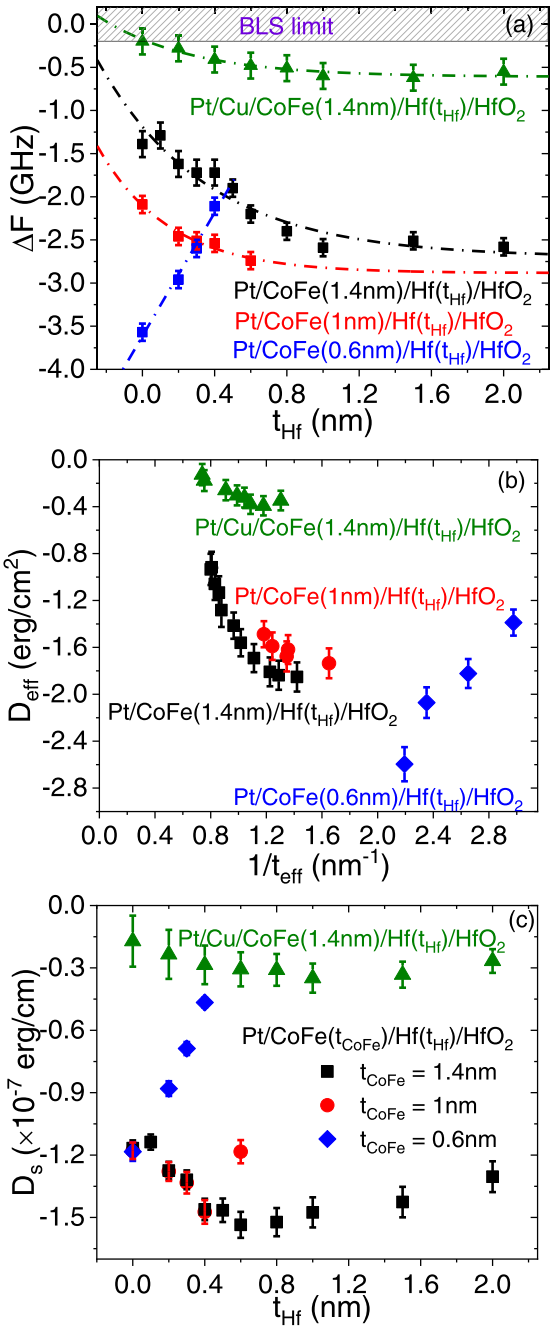

FIG. 6. (a) Hf thickness dependence of the experimental frequency mismatch ΔF measured at $k_{\text{sw}} = 20.45\ \mu\text{m}^{-1}$ for Pt/CoFe(t_{CoFe})/Hf(t_{Hf}) and Pt/Cu/CoFe(1.4 nm)/Hf(t_{Hf}) systems. Symbols refer to experimental data and dashed lines are used for eye guide. Variation of the (b) effective iDMI constant (D_{eff}) versus the inverse effective thickness of CoFe and (c) iDMI surface constant (D_s) versus the Hf thickness for Pt/CoFe(t_{CoFe})/Hf(t_{Hf}) and Pt/Cu/CoFe(1.4 nm)/Hf(t_{Hf}) systems.

requires a finite ferromagnetic thickness for its full emergence and thus its magnitude is maximized [23]. When t_{Hf} increases, t_d increases and consequently t_{eff} is reduced as mentioned above. Therefore, $|D_{\text{eff}}|$ increases due to its linear variation with $1/t_{\text{eff}}$ as suggested by Eq. (5) for sufficient t_{eff}. However, when the t_{eff} thickness is lower than a critical

value (as it is the case for Pt/CoFe(0.6 nm)/Hf(t_{Hf}) and other systems with the thicker Hf layers), $|D_{eff}|$ decreases with $1/t_{eff}$ since a finite ferromagnetic thickness for its full emergence is required [23]. Furthermore, note the significantly reduced iDMI constant by inserting Cu layer between Pt and CoFe, suggesting that Pt and CoFe atoms placed in the immediate vicinity can interact together and as Pt atoms are far away from the interface, the interaction is mediated by the spacer atoms leading to a weaker iDMI due to the weaker SOC of Cu. For Pt/Cu/CoFe/Hf(t_{Hf}), one should have nearly vanishing iDMI constant and linear variation versus with $1/t_{eff}$ if iDMI should be induced by only the Pt/CoFe interface. However, the nonlinear variation of D_{eff} with $1/t_{eff}$ for higher values of t_{eff}, suggests that the D_{eff} behavior with t_{Hf} cannot only result from the t_{eff} variation when t_{Hf} is varied and additional contribution from the upper CoFe/Hf interface should be included. This is in line with the previously observed [13] opposite sign of D_{eff} for Hf and Pt, thus leading to an additive behavior when placed on opposite sides of the ferromagnetic layer. Moreover, the extrapolation of the experimental behavior of D_{eff} versus $1/t_{eff}$, shown in Fig. 6(b), should cross zero for infinite CoFe thickness if the iDMI surface constant (D_s) is constant and thus resulting only from the Pt/CoFe interface. This allowed us to conclude that as t_{Hf} increases, the intrinsic iDMI (D_s) of the CoFe/Hf interface is stronger and thus the slope of D_{eff} versus $1/t_{eff}$ varies giving rise to this nonlinear dependence of D_{eff} and nonzero intercept. One should mention that iDMI of CoFe/Hf should saturate for a sufficiently thick Hf layer and the saturation characteristic length scale might be linked to the spin diffusion length [24].

To validate the above-mentioned hypothesis and to separate the contribution of the CoFe/Hf interface, the $M_s \times t_{eff}$ values for each t_{Hf} were used in Eq. (1) to evaluate D_s as shown in Fig. 6(c). This allows overcoming the uncertainty of both t_{eff} and M_s and thus leads to a more precise characterization of the iDMI strength. D_s should be constant if the Hf layer contributes only through the variation of t_{eff}. Therefore, as t_{Hf} increases, t_{eff} is reduced and D_s should remain constant. However, the variation of D_s versus t_{Hf}, depicted in Fig. 6(c), shows the enhancement of $|D_s|$ confirming the additive contribution of the CoFe/Hf interface which is t_{Hf} dependent owing to the required t_{Hf} for the saturation of the induced iDMI. This is in good agreement with values of D_s obtained for Pt/CoFe(0.6, 1, and 1.4 nm)/HfO_2 and for Pt/CoFe(1, and 1.4 nm)/Hf($0 \leqslant t_{Hf} \leqslant 0.4$ nm). For thicker Hf layers ($t_{Hf} > 0.4$ nm and $t_{Hf} > 0.8$ nm for $t_{CoFe} = 1$ nm and 1.4 nm, respectively), t_{eff} falls below the critical value above which the full emergence of iDMI is obtained. Therefore, $|D_s|$ decreases with increasing t_{Hf} in this range of thicknesses. This decrease of $|D_s|$ could also be related to the degradation of interfaces for ultrathin CoFe layers. Similar behavior of D_s with slightly higher t_{Hf} above which $|D_s|$ degrades, can be observed for Pt/Cu/CoFe(1.4 nm)/Hf(t_{Hf}). For Pt/CoFe(0.6 nm)/Hf(t_{Hf}), the effective thickness of CoFe is very weak and is not sufficient to the full emergence of iDMI leading to monotone decrease of $|D_s|$ when t_{Hf} increases. D_s values corresponding to $t_{Hf} = 0$ and $t_{Hf} = 0.6$ nm where the minimal and maximal $|D_s|$ are obtained allows deducing D_s values of Pt/CoFe and CoFe/Hf of $(-1.16 \pm 0.04) \times 10^{-7}$ erg/cm and $(-0.37 \pm 0.12) \times 10^{-7}$ erg/cm, respectively. The obtained D_s value for Pt/CoFe is in good agreement with the previously reported one [15]. A similar procedure can be used to deduce the D_s value CoFe/Hf interface by considering the experimental data of Pt/Cu/CoFe(1.4 nm)/Hf(t_{Hf}) systems. However, since BLS quantifies the iDMI by measuring the frequency mismatch ΔF, the lower limit of the measurable ΔF is practically limited by the frequency resolution of tandem Fabry-Perot interferometer [see Fig. 6(a)]. Therefore, BLS is more sensitive for strong iDMI values and determining the $D_s^{CoFe/Hf}$ is more reliable by using the experimental data of Pt/CoFe(1.4nm)/Hf(t_{Hf})/HfO_2.

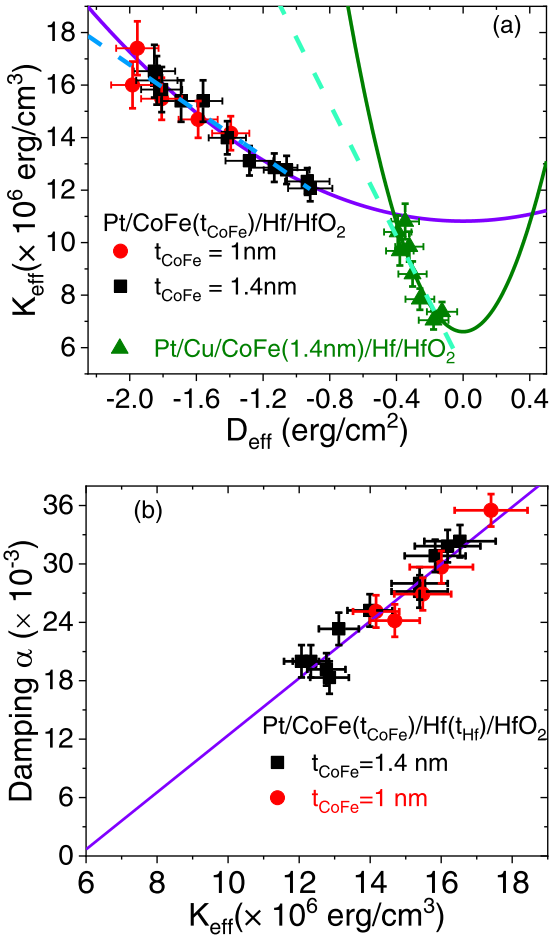

FIG. 7. (a) Variations of the perpendicular effective magnetic anisotropy constant (K_{eff}) as a function of the effective iDMI constant (D_{eff}) for Pt/CoFe(t_{CoFe})/Hf(t_{Hf}) and Pt/Cu/CoFe(1.4nm)/Hf(t_{Hf}) systems with a variable Hf thickness. Symbols refer to experimental data, dashed lines are linear fits and the solid lines are fits with equations: $K_{eff} = 1.08 \times 10^7 + 0.16 \times 10^6 D_{eff}^2$ (violet line) and $K_{eff} = 0.66 \times 10^6 + 2.59 \times 10^7 D_{eff}^2$ (green line). (b) Variations of the damping constant (α) as a function of the effective PMA constant (K_{eff}) for Pt/CoFe(t_{CoFe})/Hf(t_{Hf}) system with a variable Hf thickness. Symbols refer to experimental data and solid lines are linear fits.

The correlation between iDMI, PMA, and damping was also investigated for Pt/CoFe(1.4 and 1 nm)/Hf(t_{Hf}) and Pt/Cu/CoFe(1.4nm)/Hf(t_{Hf}) by plotting K_{eff} as a function of D_{eff} and α versus K_{eff} as shown in Fig. 7. Due to the degradation of D_{eff} for Pt/CoFe(0.6 nm)/Hf(t_{Hf}), this

system is not considered for the correlation investigation. Figure 7(a) revealed a quadratic dependence of K_{eff} versus D_{eff} as theoretically predicted from perturbation theories for PMA [25] and iDMI [26], where iDMI energy results from the first order of the SOC, while the PMA comes from the second order. However, a linear correlation between K_{eff} and damping was obtained due to the second-order dependence of the two parameters with SOC as expected theoretically. This correlation suggests the common interfaces involved in these three SOC-related effects.

It is worth mentioning that while quadratic or linear dependences of K_{eff} versus D_{eff} are conceivable in the case of Pt/Cu/CoFe(1.4 nm)/Hf(t_{Hf})/HfO_2, a quadratic fit is more convenient and fits better with the experimental data for the case of Pt/CoFe(1.4 nm)/Hf(t_{Hf})/HfO_2, as shown in Fig. 7(a). By varying the Hf thickness, the SOC at the CoFe/Hf interface is more affected for Pt/Cu/CoFe(1.4 nm)/Hf(t_{Hf})/HfO_2 systems due to intermixing at this interface and thus the theoretical expected quadratic correlation is more likely to be achieved. Moreover, in the Pt/CoFe(1.4 nm)/Hf(t_{Hf})/HfO_2 system, the two interfaces with CoFe contribute differently to D_{eff} and K_{eff}: while the contribution of both Pt/CoFe and CoFe/Hf interfaces for K_{eff} is significant, iDMI results mainly from the Pt/CoFe interface. In contrast, only the CoFe/Hf interface is responsible for both iDMI and PMA in the Pt/Cu/CoFe(1.4 nm)/Hf(t_{Hf})/HfO_2 system. This might explain the different correlation between K_{eff} and D_{eff} in the two systems.

IV. CONCLUSION

A detailed study of the PMA, iDMI, and Gilbert damping constants for Pt/CoFe(t_{CoFe})/Hf(t_{Hf})/HfO_2 with $t_{CoFe} = 0.6$, 1 and 1.4 nm and Pt/Cu/CoFe(1.4nm)/Hf(t_{Hf}) HfO_2 where t_{Hf} varies in the range 0–2 nm*s*, was conducted. A simple picture which considers that varying the Hf thickness results in the variation of the effective thickness of CoFe allows us to explain the main observed trends. Indeed, when varying Hf thickness, the magnetic dead layer at the CoFe/Hf interfaces increases, reducing the effective thickness of CoFe and leading to higher damping due to spin pumping, which was found to be induced mainly by the Pt/CoFe interface. Moreover, the effective thickness dependence of the effective PMA constant revealed the existence of two regimes where the increase of K_{eff} with thickness in both regimes is consistent with the decrease of the CoFe effective thickness as t_{Hf} increases. The total PMA is found to result from surface and volume contributions where CoFe/Hf and Pt/CoFe interfaces are the main sources. BLS measurements showed that the iDMI enhancement with increasing t_{Hf} cannot only result from the CoFe effective thickness variation when t_{Hf} is varied and additional contribution from the upper CoFe/Hf interface should be included. This is consistent with the previously observed opposite iDMI sign for Hf and Pt, thus leading to an additive behavior when they are placed on opposite sides of CoFe. Indeed, as t_{Hf} increases, the intrinsic iDMI of the CoFe/Hf interface is maximum when $t_{Hf} = 0.6$ nm. By combing the obtained values for the minimal and maximal surface iDMI constants (D_s) corresponding to $t_{Hf} = 0$ and $t_{Hf} = 0.6$ nm, we deduced the D_s constants of Pt/CoFe and CoFe/Hf interfaces, estimated to be $(-1.16 \pm 0.04) \times 10^{-7}$ erg/cm and $(-0.37 \pm 0.12) \times 10^{-7}$ erg/cm, respectively. Quadratic correlation between k_{eff} and D_{eff} and linear dependence of damping constant α versus K_{eff} were evidenced.

ACKNOWLEDGMENTS

This work has been supported by the Conseil regional d'Île-de-France (convention 1763) through the DIM NanoK (BIDUL project). R.B.M., M.N., and M.S.G. acknowledge the financial support for this work from MRID, CNCS/CCCDI – UEFISCDI, through Grant No. PN-III-P4-ID-PCE-2020-1853, SPINSYNE.

[1] A. Crépieux and C. Lacroix, J. Magn. Magn. Mater. **182**, 341 (1998).
[2] M. J. Benitez, A. Hrabec, A. P. Mihai, T. A. Moore, G. Burnell, D. McGrouther, C. H. Marrows, and S. McVitie, Nat. Commun. **6**, 8957 (2015).
[3] S. D. Pollard, J. A. Garlow, J. Yu, Z. Wang, Y. Zhu, and H. Yang, Nat. Commun. **8**, 14761 (2017).
[4] M. Hervé, B. Dupé, R. Lopes, M. Böttcher, M. D. Martins, T. Balashov, L. Gerhard, J. Sinova, and W. Wulfhekel, Nat. Commun. **9**, 1015 (2018).
[5] L. Schmidt, J. Hagemeister, P.-J. Hsu, A. Kubetzka, K. von Bergmann, and R. Wiesendanger, New J. Phys. **18**, 075007 (2016).
[6] J. Sampaio, V. Cros, S. Rohart, A. Thiaville, and A. Fert, Nat. Nanotech. **8**, 839 (2013).
[7] W. Jiang, P. Upadhyaya, W. Zhang, G. Yu, M. B. Jungfleisch, F. Y. Fradin, J. E. Pearson, Y. Tserkovnyak, K. L. Wang, O. Heinonen, S. G. E. Velthuis, and A. Hoffmann, Science **349**, 283 (2015).
[8] K. S. Ryu, L. Thomas, S. H. Yang, and S. Parkin, Nat. Nanotechnol. **8**, 527 (2013).
[9] S. Mangin, D. Ravelosona, J. Katine, M. Carey, B. Terris, and E. E. Fullerton, Nat. Mater. **5**, 210 (2006).
[10] S. Ikegawa, F. B. Mancoff, J. Janesky, and S. Aggarwal, IEEE Trans. Elec. Dev. **67**, 1407 (2020).
[11] R. Sbiaa, S. Y. H. Lua, R. Law, H. Meng, R. Lye, and H. K. Tan, J. Appl. Phys. **109**, 07C707 (2011).
[12] P.-H. Jang, K. Song, S.-J. Lee, S.-W. Lee, and K.-J. Lee, Appl. Phys. Lett. **107**, 202401 (2015).
[13] R. Soucaille, M. Belmeguenai, J. Torrejon, J.-V. Kim, T. Devolder, Y. Roussigne, S.-M. Cherif, A. A. Stashkevich, M. Hayashi, and J.-P. Adam, Phys. Rev. B **94**, 104431 (2016).
[14] C.-F. Pai, M.-H. Nguyen, C. Belvin, L. H. Vilela-Leão, D. C. Ralph, and R. A. Buhrman, Appl. Phys. Lett. **104**, 082407 (2014).
[15] M. Belmeguenai, M. S. Gabor, Y. Roussigné, A. Stashkevich, S. M. Chérif, F. Zighem, and C. Tiusan, Phys. Rev. B **93**, 174407 (2016).

[16] C.-F. Pai, Y. Ou, L. H. Vilela-Leão, D. C. Ralph, and R. A. Buhrman, Phys. Rev. B **92**, 064426 (2015).
[17] M. Belmeguenai, J.-P. Adam, Y. Roussigné, S. Eimer, T. Devolder, J.-V. Kim, S. M. Cherif, A. Stashkevich, and A. Thiaville, Phys. Rev. B **91**, 180405(R) (2015).
[18] M. T. Johnson, P. J. H. Bloemen, F. J. A. den Broeder, and J. J. de Vries, Rep. Prog. Phys. **59**, 1409 (1996).
[19] J. M. Shaw, H. T. Nembach, and T. J. Silva, Phys. Rev. B **85**, 054412 (2012).
[20] M. Belmeguenai, M. S. Gabor, F. Zighem, and C. Tiusan, J. Phys. D **50**, 135002 (2017).
[21] R. Weber, D.-S. Han, I. Boventer, S. Jaiswal, R. Lebrun, G. Jakob, and M. Kläui, J. Phys. D **52**, 325001 (2019).
[22] Y. Li, F. Zeng, Steven S.-L. Zhang, H. Shin, H. Saglam, V. Karakas, O. Ozatay, J. E. Pearson, O.-G. Heinonen, Y. Wu, A. Hoffmann, and W. Zhang, Phys. Rev. Lett. **122**, 117203 (2019).
[23] Y.-K. Park, J.-S. Kim, Y.-S. Nam, S. Jeon, J.-H. Park, K.-W. Kim, H.-W. Lee, B.-C. Min, and S.-B. Choe, NPG Asia Mater. **12**, 38 (2020).
[24] S. Tacchi, R. E. Troncoso, M. Ahlberg, G. Gubbiotti, M. Madami, J. Åkerman, and P. Landeros, Phys. Rev. Lett. **118**, 147201 (2017).
[25] P. Bruno, Phys. Rev. B **39**, 865 (1989).
[26] M. Heide, G. Bihlmayer, and S. Blügel, Physica B **404**, 2678 (2009).